

## **Development of Powder Diffraction Analysis Tools for a Nanocrystalline Specimen:**

### **An Emphasis upon NiTi (Nitinol)**

Erich Owens

Office of Science, SULI Program

Albion College

Stanford Linear Accelerator Center

Menlo Park, California

August 25<sup>th</sup>, 2006

Prepared in partial fulfillment of the requirements of the Office of Science, U.S. Department of Energy Science Undergraduate Laboratory Internship (SULI) Program under the direction of Dr. Apurva Mehta of the Stanford Synchrotron Radiation Laboratory (SSRL) at the Stanford Linear Accelerator Center (SLAC).

Participant:

\_\_\_\_\_  
Signature

Research Advisor:

\_\_\_\_\_  
Signature

## **Table of Contents**

Abstract	iii
Introduction	1
Materials and Methods	2
Results and Discussion	3
Conclusions	6
Acknowledgements	7
References	7
Figures	8

## **ABSTRACT**

**Development of Powder Diffraction Analysis Tools for a Nanocrystalline Specimen: An Emphasis upon NiTi (Nitinol). ERICH OWENS (Albion College, Albion, MI 49224)**

**MATTHEW STRASBERG (Cornell University, Ithaca, NY 14850) APURVA MEHTA (Stanford Linear Accelerator Center, Menlo Park, CA 94029), SAMUEL WEBB (Stanford Linear Accelerator Center, Menlo Park, CA 94029)**

Powder diffraction is a specialized technique whose investigatory limits are constrained by the scale of the crystallized substance being scanned versus the probe beam used. When disparate in scale, with the photon spot size larger than the crystal being probed, many are employed, the resulting diffraction image being cast from all possible incident angles, constructing  $\chi$ -arcs containing information about the crystalline structure of the material under examination. Of particular interest to our collaboration is the structure of Nitinol, a superelastic Nickel-Titanium alloy, whose phase transformations and load bearing deformations can be studied by usage of diffraction, with wide sweeping biomedical uses. Analysis of this data is complicated by phase transformation and material fluorescence, which make difficult the computational modeling of the peaks within concentric  $\chi$ -arcs. We endeavored to construct a series of computational tools (the amalgamation of them known as 2DPeakFinder) for refining and extracting this relevant data, toward the end of employing previously developed algorithms in the material's structural analysis. We succeeded to a large degree with the use of an iterative algorithm to navigate radial complexity of the signal and manage to retain a distinction between useful signal and superfluous background noise. The tools developed in this project are a small step in readily streamlining the analysis and physical modeling of a Nanocrystalline material's structural properties.

## INTRODUCTION

Visual inspection is the most direct way to examine an item's structure. When it comes to molecular arrangements, however, the visible light spectrum fails us as its associated wavelengths are too large to probe the microscopic structures we're concerned with. Higher energy photons (namely, x-rays), having thus smaller wavelengths, must therefore be employed. A complication emerges when the size of the probe beam is larger than the grain-size of the sample, exposing many different crystal orientations resulting in diffraction arcs or rings. Techniques and tools for interpretation of this "smeared" diffraction patterns – often called powder pattern-- are thus necessary. This necessity is acute when investigating nano-crystalline materials, as it is not yet possible to make sufficiently intense x-ray probes of nanometer dimensions. There a wealth of information contained in these powder diffraction patterns. For example, Bibee in 2005 [3], showed that it is possible to extract the full strain tensor from the distortion of diffraction rings in a 2D powder diffraction pattern—our collaboration refined these mathematical relationships [2]. It also appears possible to extract crystallite orientation information, commonly referred to as sample texture, from a 2D powder diffraction pattern. This relevant information is accessible within the bright arc fringes of a diffraction image (see figure 1), particularly the location of these fringes' peak intensity, location of said peak from a determined center, as well as the relative width of these fringes. We refer to the azimuthal angle as  $\chi$ , and the radial angle  $2\theta$  as consequence of Bragg's law:

$$\lambda = 2d \sin[\theta]$$

Q subsequently is defined as the geometric relation between  $2\theta$  detailed below and can be interpreted visually as the radial distance.

$$Q = 4\pi \sin(\theta) / \lambda$$

A material when subjected to load will strain. The macroscopic deformation of the material can arise from many different mechanisms at a microscopic level and can be easily distinguished by a diffraction experiment. The microdeformation can be due to elastic deformation of the atomic bonds. This type of deformation results in distortion of the powder rings, as shown by [1]. The microdeformation can be also due to creation of dislocations, or slip on 'slip planes'. This form

of deformation results in broadening of powder rings. In some very heavily twinned (highly texturized with a clear bipolar distribution of intensities by value of  $\chi$ ) material the microdeformation can be due to transformation of one set of twins into another mechanical more favorable form. This type of microdeformation changes the texture of the sample and hence redistributes the location of bright fringe intensity in a diffraction ring.

We propose to develop various software tools and techniques for powder diffraction analysis that will easily and quickly extract diffraction peak position, width, and intensity information as a function of the azimuthal  $\chi$  angle. We will apply these tools to understand deformation of Nitinol, which exhibits all three modes of microstrains [2].

## **MATERIALS AND METHODS**

### *Diffraction and Data Collection*

The powder diffraction data utilized was collected by Apurva Mehta and collaborators from Nitinol Devices & Components (hereafter NDC). Thin strips in a dogbone conformation were measured with constant incident angle with the routine powder method [1]. The strips were pulled in a tensile strain-inducing rig until critical fracture. The diffractometer was newly calibrated at each load increment.

### *Processing of Signal*

The 2D raw data files as collected by the diffractometer are more easily worked in diffraction related coordinate space instead of a Cartesian pixel space. The collected images resemble a series of continuous, concentric rings and arcs. Program Fit2D [4] was used to transform these images into the diffraction coordinates of  $Q$  and  $\chi$  (figure 2).

The newly processed data sets present a series of rows representing  $\chi$ , with a characteristic central peak of high relative intensity to the surrounding intensity values (figure 6). The primary problem presented is then distinguishing background from signal. These lesser range of intensities may be referred to as background, and for our purposes detract from the desired data describing the central peak, which we'll call signal. This may be specified by a user, however as

viewed in figure 2, there is not a common range for signal along all values of  $\chi$ . Exhaustive specification of this range by the use is possible, but time intensive, so efforts are to be made in automating this process. Background intensity is a common artifact in diffraction patterns, resultant often from material fluorescence, scattering from the air in the collimator and beam stop, or diffuse scattering resulting from crystal imperfections [1]. The problem then posed is detecting this background intensity level, determining its characteristic distribution (constant, linear, or more complex relationship) then subtracting in some fashion from the data. At this point some mathematical function may be modeled to fit the remaining central peak, with goodness of fit and residue between it and that modeled used to gauge the success of such a process. The use in having such a model is that the peak's intensity, location and width may then easily be calculated for exportation.

## RESULTS AND DISCUSSION

### *Overview*

A successful scheme was developed to address an iterative approach toward processing the caked (integrated along axes of  $\chi$  and  $Q$ , which are polar coordinates in the pixel space the image was taken in) diffraction patterns. The program developed will hereafter be referred to as “2DPeakFinder”. The first  $\chi$  row is displayed to the user as a cross section in pixel space. He or she is prompted to input the range to search for the desired peak. A mean is calculated of the background, and is subtracted from the signal and the data outside the user's specified range is nullified. A Gaussian fit is made with three determined coefficients, in the form of:

$$a_1 e^{-((x-b_1)/c_1)}.$$

This sufficing as our employed mathematical fitting model. The fit's peak location (corresponding to  $b_1$ ), peak intensity( $a_1$ ), and peak width( $c_1$ ) is recorded for later file output. The determined range for the row is used for the next, but the location of the next row's half-maxima (allowing for calculation of the Gaussian distribution's width) as they deviate from the previous row readjusts the program's peak search range. This is repeated onwards. The results may be appreciated qualitatively in figures 2 through 5, the second set projected upon a false z-

axis representing intensity. The data recorded to a separate file is converted to values of  $Q$  and scaled against  $\chi$ , as referenced by an external file set by the provider of caked data with reference to what the range of appropriate values are. That data included are column vectors of the fitted rows' Gaussian peak intensities, peak widths, and peak location, ran against a steadily increasing index reflective of which  $Q$  value these correspond to.

### *Background and Signal*

With the underlying assumption that the program precedes upon, that some data is essentially background and the rest relevant signal (contained within one peak). Within the algorithm, the assumption results in a strict demarcation of this with two variables storing the endpoints of this range. Complications therefore arise with the presence of supernumerary diffraction lines (manifested as peaks in the row space the data is processed), often resulting from cell distortion and phase transformations [1]. Figure 6 is a cross-section of caked austenite diffraction data, around  $Q = 29$ , along  $\chi = -59$  (this was chosen as representative of most of the data this program intends to process, at least with regard to austenite samples, with the most possible complexity the authors have seen). The supernumerary peaks are clearly visible. Figure 7 outlines the cross section seen in 5 ( $\chi = -179$  around  $Q = 29$  for a relative macrostrain of 500 micrometers) with a few added dimensions. The background calculation was based on a mean calculation, yielding a constant value to be subtracted. The resulting data was then nullified (set to zero) at all points except the range indicated to be signal. Due to the negation of the outside regions of the signal, if relevant signal is within the cutoff region as is used for a naïve fit then it would not contribute to the determination. The inherent assumption in this approach does not accommodate for complex background patterns that may vary by value of  $Q$  [1]. Similarly, the data sets encountered in development of 2DPeakFinder were revealed to be polluted by Martensitic imperfections, whose presence create supernumerary peaks adjacent to the central desired one (see figure 6), whose presence we both do not desire in calculation of a constant mean (not representative of a constant additional signal to our relevant peak) but whose presence casts inaccuracies in the curve fitting (figure 10). The authors suggest a more complex scheme, whose approach fundamentally differs in selecting not a binary state of good or bad data sections, but rather a series of points indicating representative background data points, then

relying upon a cubic interpolating spline distribution fit upon these to subtract out a suitably complex model.

### *Peak Shape*

A Gaussian fit was employed for the current version of 2DPeakFinder, however an examination of the residue of this fit (between the background negated signal as determined by the iterative algorithm and the three coefficient fit as employed by the 'fit' function of the Matlab Curve Fitting Toolbox [5], see Figure 10) reveal it is not entirely representative of the peak we intend to fit. The clear deficiency appears toward the base of the distribution, implying greater accuracy with usage of a Lorentzian/Cauchy distribution, whose characters shape is that with a wider and longer trailing tail than the Gaussian/Doppler profile. Preferably some convolution of the two, known as a Voigt distribution should be employed. Examination of the residue in detail allows for determination of goodness of fit, among other things, and thus is computed by 2DPeakFinder (Figures 8 and 9). The primary goal of our collaboration's study of Nitinol is extraction of the strain tensor, which is primarily fueled by the location of peaks, secondarily from the distribution of intensities (which is used as a weighting factor in the determination of the tensor) . Thus the discrepancies between the original data's maximum value in the peak search range and the Gaussian fit's peak location, as well as the relative intensities of the fits to the original data convey important information about the goodness of our model. We calculated the deviation between the maximum points of the original data set of Austenite data centered around  $Q = 42$  at 440 relative micrometers of strain, and that of the fit's peak locations, and encountered surprising results. There was presented a mean deviation of 1.6685 pixels (see figures 13 and 14). This is statistically significant and indicative of a standard asymmetry to the peaks in the data set that was not previously understood. A more robust fitting system would accommodate the data and fit for this. Further investigations too are required as to whether this is the true nature of the prominent signal peak or contribution from sample-specific Martensitic phase pollution.

### *Transitioning from 1D to 2D: Iterative Approach*

The  $\chi$  rings we've been examining are not perfect circles. When radially transformed into the caked images we're familiar with (Figure 2) this results in a contour indicative of the elliptical



nature of the  $\chi$ -valued intensities. As a result, a specified range for signal against background cannot be fixed, but rather adaptive. From a practical standpoint, is not time effective for a user to define these ranges for every value of  $\chi$  for each Q-focused caked image for each set of strained and location specific data. Rather, 2DPeakFinder takes a user inputted declaration of the range of relevant signal for the first row in pixel space of the data. It follows the steps described earlier in the paper, and fits this. It uses the same range for the next row down using the same specifications for the signal range. However, after this point the disparity between its peak location and the peak location of the row before it is calculated, this value used to adjust the range values left or right as needed. The underlying assumption then is of direct continuity in the  $\chi$ -ring and expectation of small shifts by Q of relevant signal per row in pixel space. The former case is encountered when we use 2DPeakFinder to process caked data focused upon  $Q = 51$  at high stress levels, as a result of shadowing from the grips used to apply the relative strain, about  $500\text{ }\mu\text{m}$  or above (Figures 11 and 12). The missing data poses a problem for the iterative algorithm, which operates off the assumption of direct continuity. Table 1 details the progression of the fits made and the problems encountered within the data. Around  $\chi = -35$  the data begins to be shadowed. This results in missing background signal; subsequently the calculated mean is an underestimate of the data we'd expect. As a result, the fitted peak in a row with missing background will possess overestimated peak intensity. As the shadow in the data engulfs the actual relevant signal (as can be interpolated), the iterative algorithm begins to fit a false peak that then corresponds solely of the remaining background juxtaposed with the nullified remainder of the data (see  $\chi = 0$  in Table 1). When the shadowing diminishes and the signal properly reappears, due to the slight adjustments within the range of the iterative algorithm in fitting data and reevaluating the proper range for signal, there is significant lag displayed in returning to proper values (see  $\chi = 25$  in Table 1).

## CONCLUSIONS

The fits constructed by the developed program 2DPeakFinder appear accurate within the most general considerations. Their application to the analysis of diffraction data is specific and robust for that which has continuity within all values of  $\chi$ , and where usable signal is interpreted to be a symmetric distribution which is evenly separated from undesirable constant background by a simple specification of a single range. Within this paper we presented for your consideration

cases where these assumptions failed, and a detailed analysis of those events. The iterative approach was largely successful, and minimized user input. Future approaches would consider largely more complex background regression models, routines to compensate for shadowed or missing data-- which our algorithm managed to traverse only for virtue of there existing some remaining background for it to fit. Despite this, there was significant lag in its response to modeling existent data once it encountered true data again, and that is to be minimized. Also of particular import would be determination of the most appropriate mathematical model used in fitting the central peaks within our data. The studies of calculated residue and deviations indicated both a general inadequacy of the Gaussian distribution, due to the broader base of the actual signal and its apparent asymmetry.

### **ACKNOWLEDGEMENTS**

I'd like to thank Apurva Mehta for his role as my mentor this summer, I learned more about the continuing process of science and its communication than I thought possible. I'd also like to thank my collaborator and friend Matthew Strasberg for his role in these projects this summer, as well as the contributions of Samuel Webb, Monica Barney, and David Bronfenbrenner. Thank you as well to Stephanie Majewski for her valuable assistance. Also of importance are the facilities of the Stanford Synchrotron Radiation Laboratory, the Stanford Linear Accelerator Center, and the Office of Science through the Department of Energy for making all of this possible.

### **REFERENCES**

- [1] B.D. Cullity, S.R. Stock Elements of X-Ray Diffraction, 3e. New York: Prentice Hall, 2001.
- [2] M. Strasberg, "Determining Micromechanical Strain in Nitinol" Office of Science, SULI Program, Stanford Linear Accelerator Center, Menlo Park, CA. Tech. Rep. August 18, 2006.
- [3] M. Bibee, "Mapping Strain in Nanocrystalline Nitinol: an X-ray Diffraction Method." Office of Science, SULI Program, Stanford Linear Accelerator Center, Menlo Park, CA. Tech. Rep. August 19, 2005.

[4] Dr. Andy Hammersley, The European Synchrotron Radiation Facility, “The Fit2D Home Page” August 2006, <http://www.esrf.fr/computing/scientific/FIT2D/>

[5] The Mathworks Inc, “MATLAB Manual”, August 2006,  
<http://www.mathworks.com/access/helpdesk/help/techdoc/matlab.shtml>

## FIGURES AND TABLES

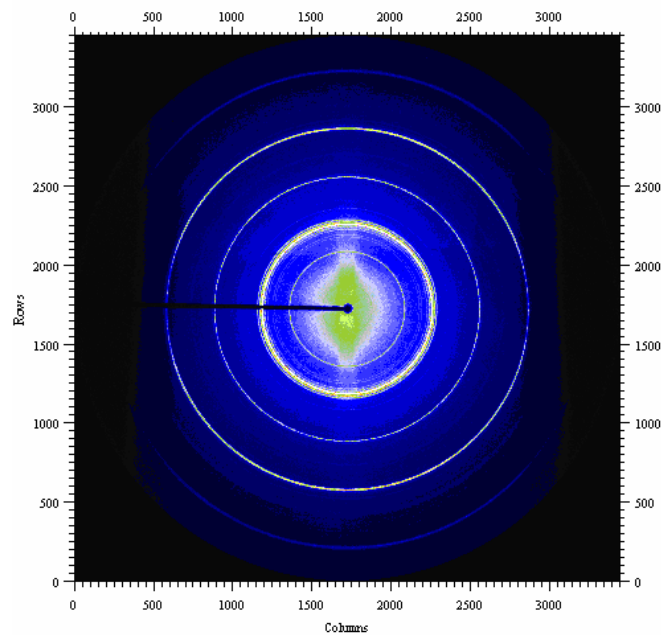


**Figure 1 - Diffraction Image of Nitinol in Martensite Phase under load. Note the characteristic bright fringes arranged in mostly continuous & concentric arcs.**

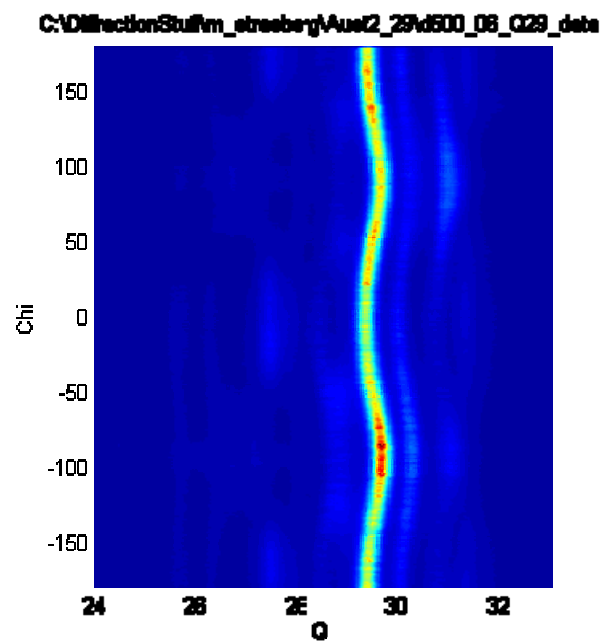


Figure 2 - Caked Ring, Top-down false color image

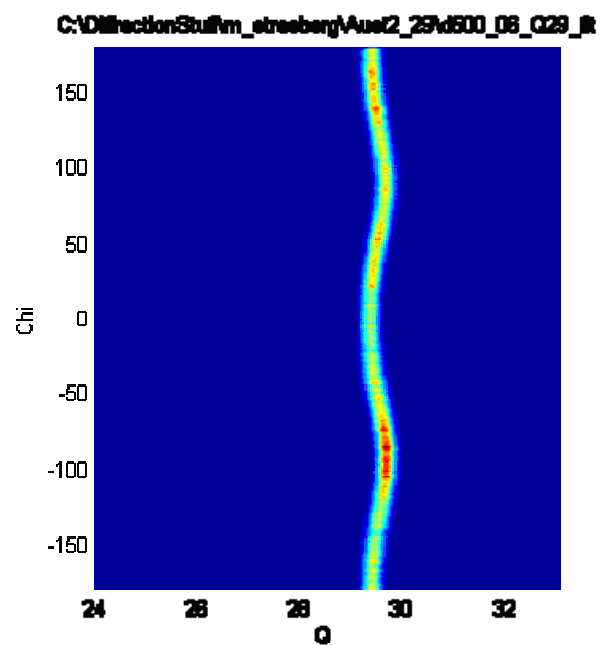


Figure 3 - Caked ring, processed with the developed iterative algorithm, Top-down false color image.

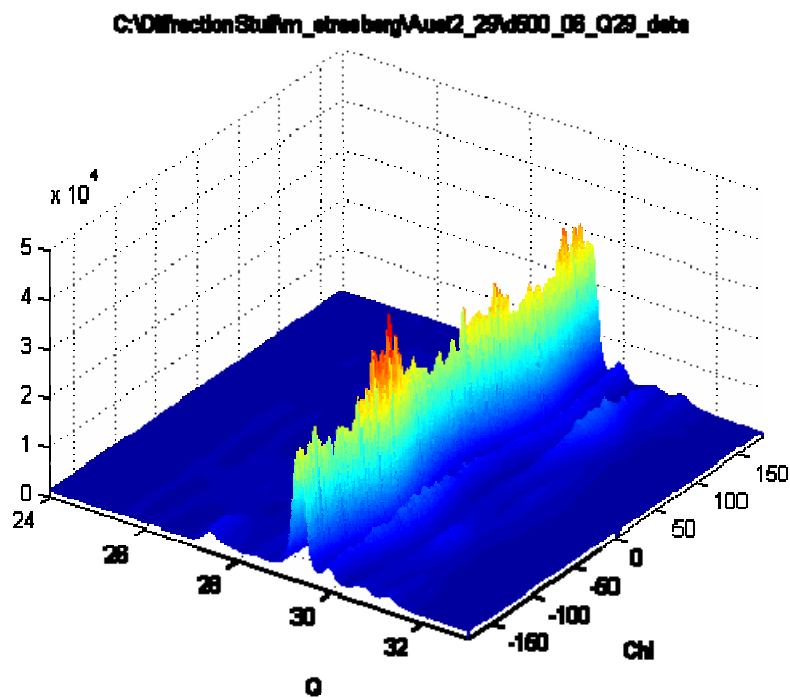


Figure 4 - (45 deg, 35 deg) view of false color/false axised unprocessed data

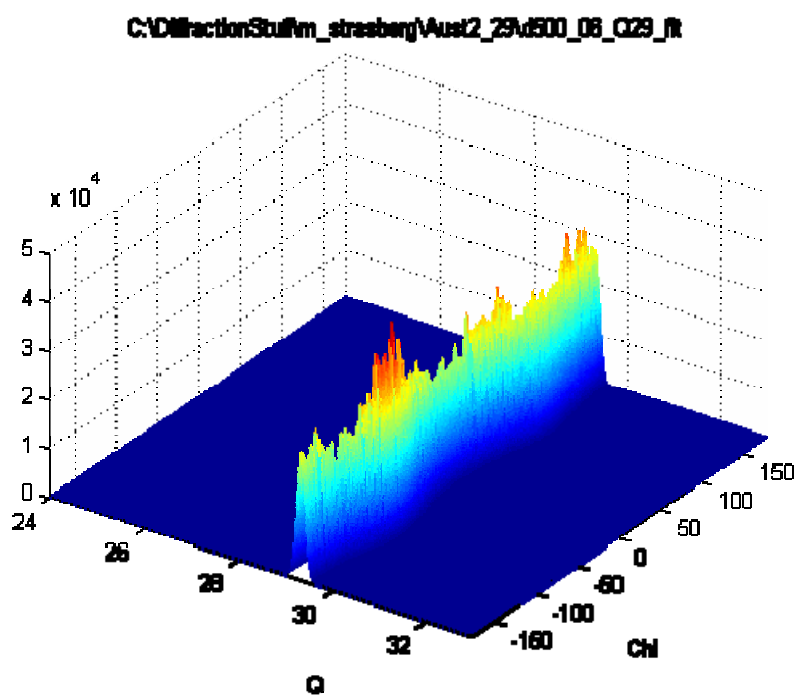
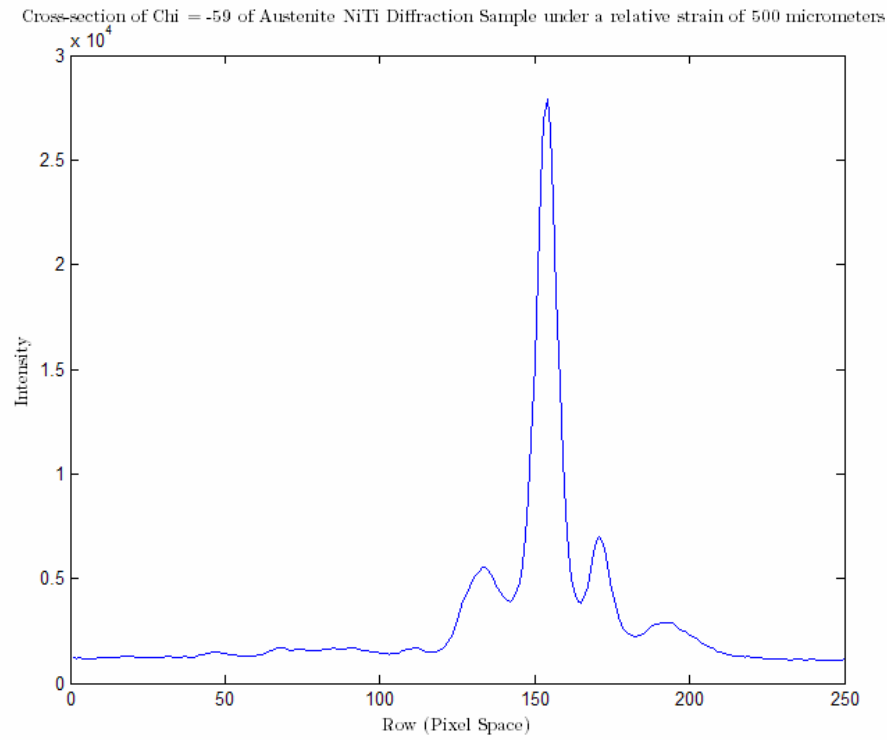
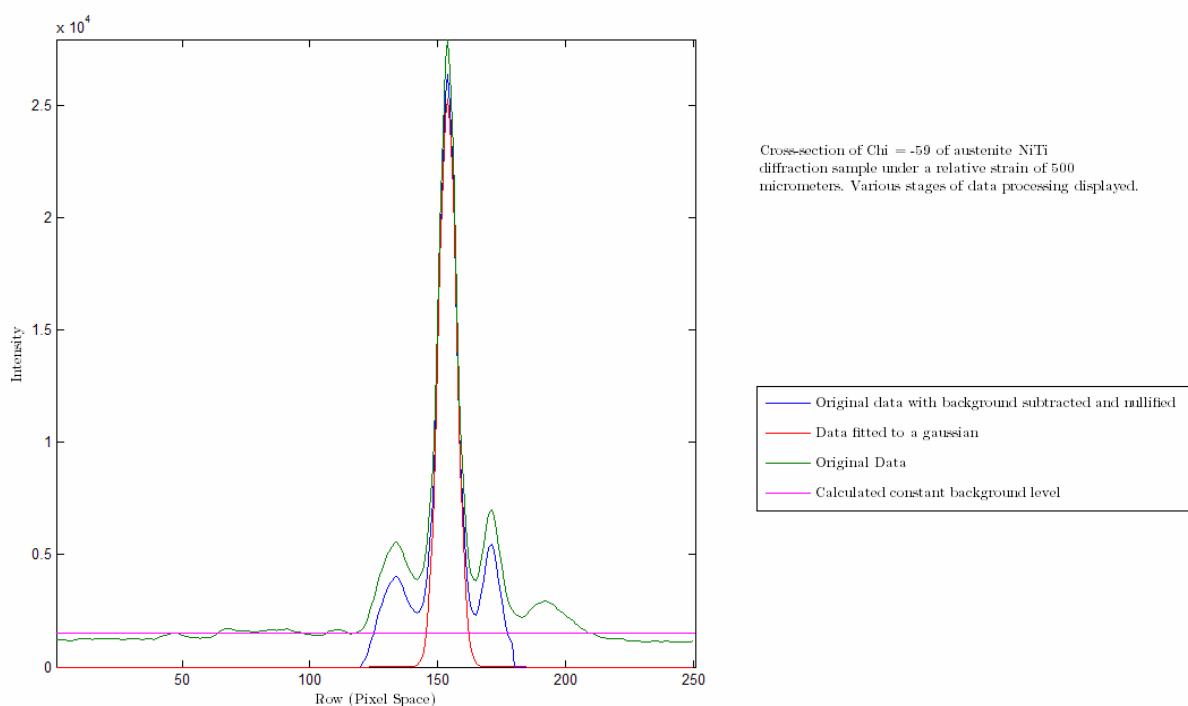


Figure 5 - (45 deg, 35 deg) view of a false color/false axised processed data



**Figure 6 - NiTi in Austenite phase diffraction sample cross section. The sample is under a relative strain of 500 micrometers. The image is data focused along  $Q = 29$  along  $\chi = -59^\circ$ . Note the multiple peaks in addition to the prominent central peak.**



**Figure 7 - Similar to Figure 5, but now showing the various stages of file processing. Original data minus displayed constant calculated background, as well as the subsequent fit.**

Residue of fit for diffraction data of NiTi Austenite around  $Q = 29$  at 500 micrometers of relative strain

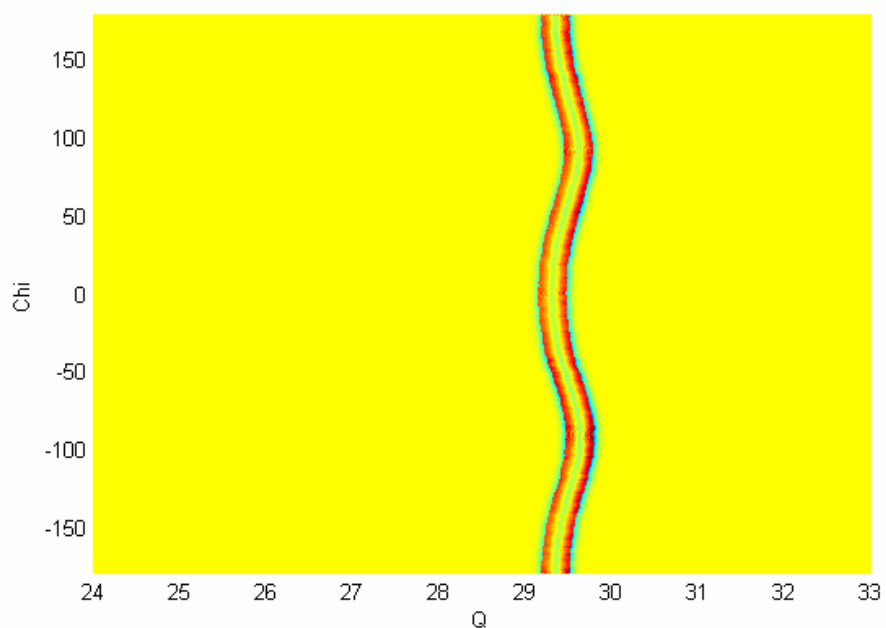


**Figure 8 - Residue, top-down false colored view**

Residue of fit for diffraction data of NiTi Austenite around  $Q = 29$  at 600 micrometers of relative strain

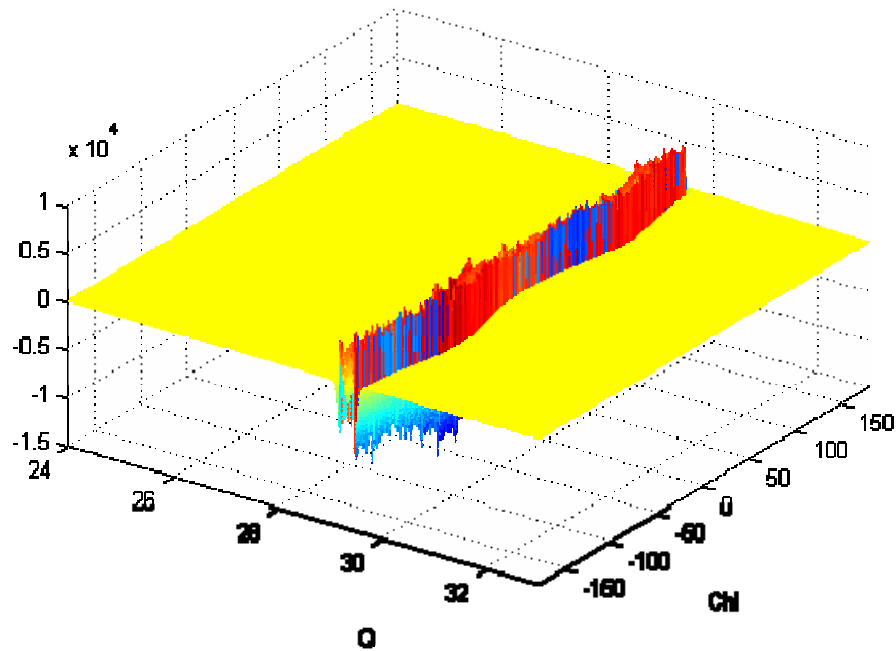


Figure 9 – Residue from processed data of 500 micrometers of relative strain around  $Q = 29$ , (35,45) degree view

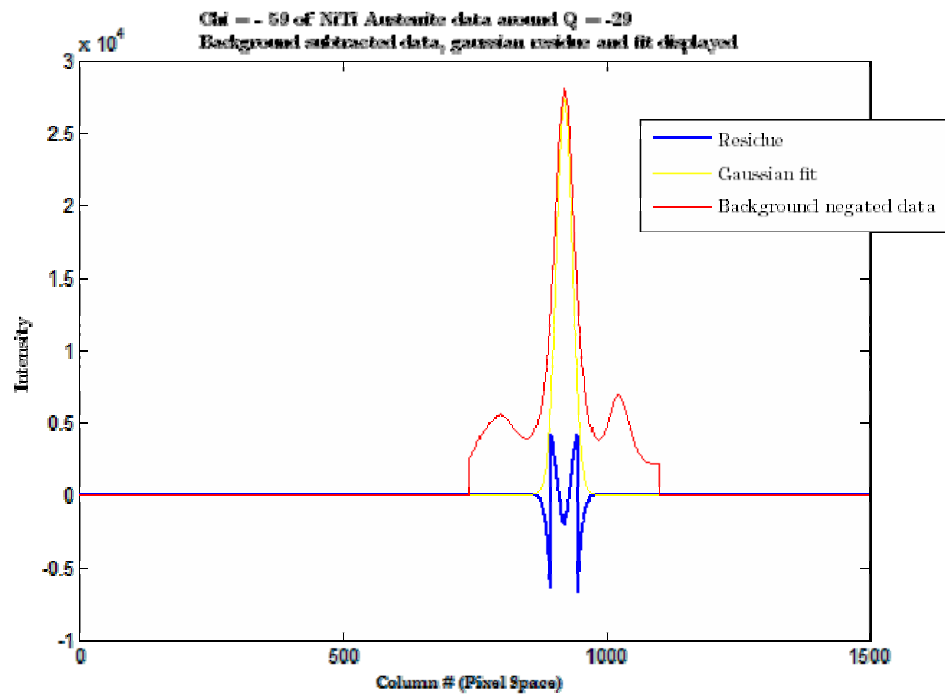


Figure 10 - Cross-section displaying negated background, a Gaussian fit, and the residue.



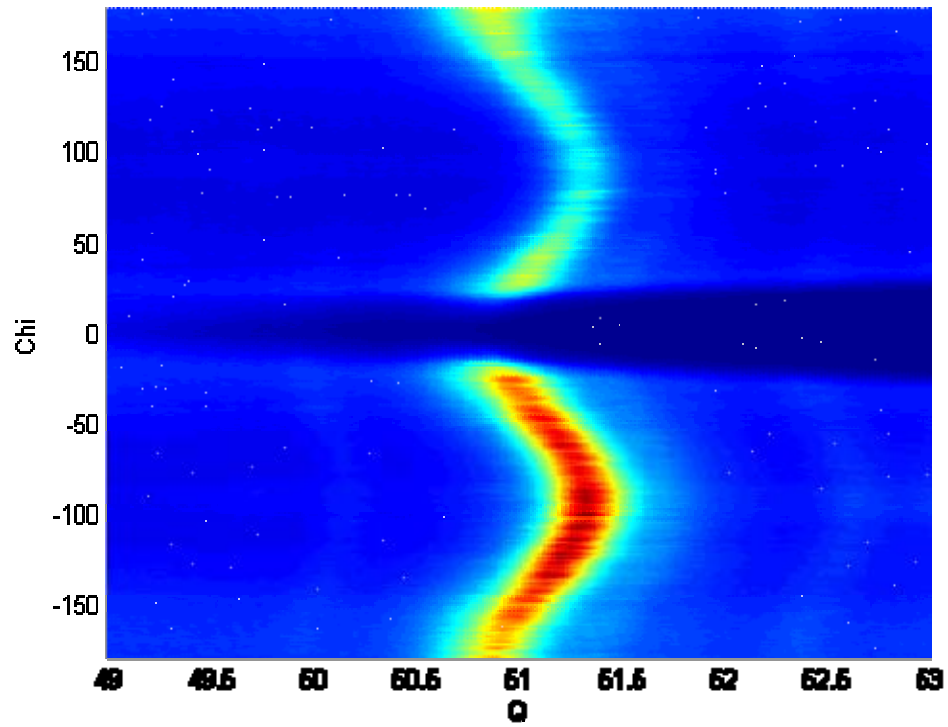


Figure 11 - Example of shadowing in high strain (500 micrometers) data around  $Q = 51$ .

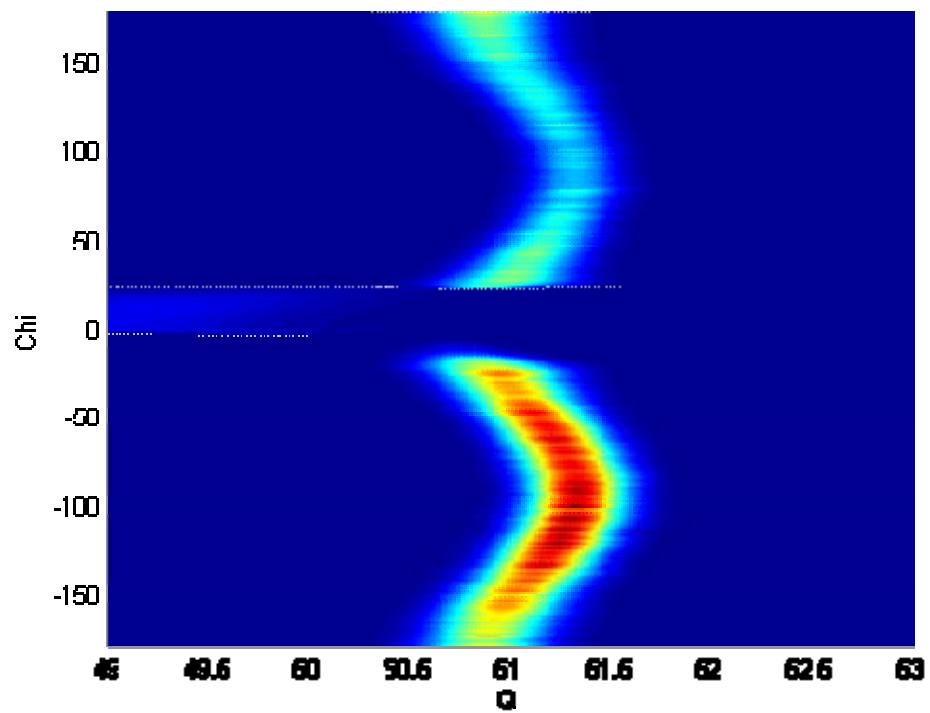


Figure 12 - Fit of shadowing case, note the fits to erratic background within the discontinuity

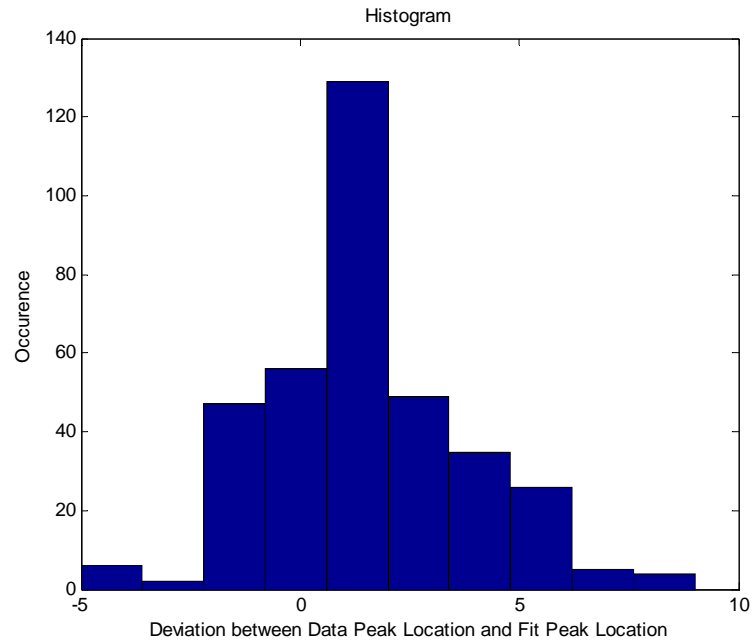


Figure 13 - Histogram displaying deviation in peak locations between the data set and the fit of arbitrarily chosen Austenite Chi ring around  $Q = 42$  at 440 micrometers of relative strain

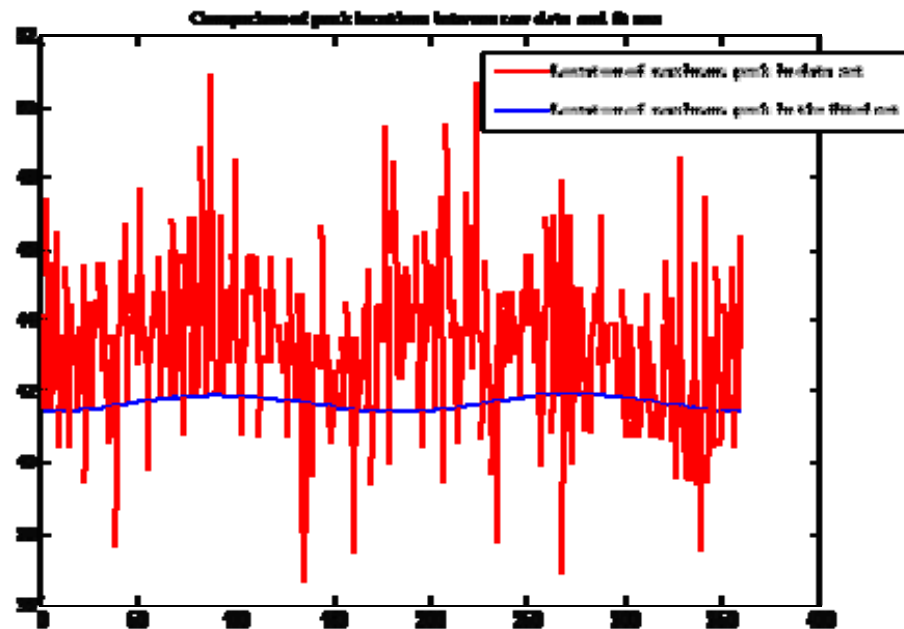
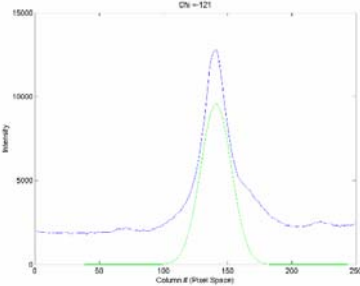
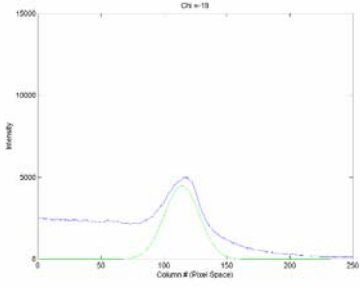
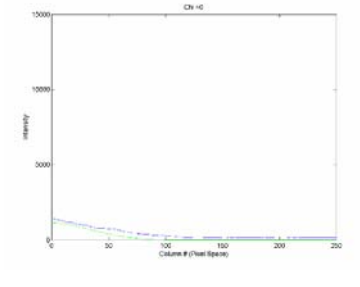
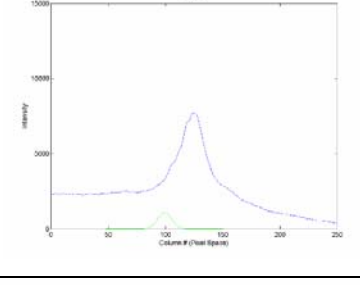
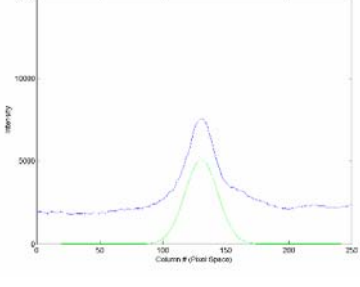


Figure 14 - Comparisons of the peak locations between raw data and fit sets. Note the general shift and asymmetry of the difference. Units are in pixel space.

**Table 1 - Selected cross sections of data centered around  $Q = 51$  for high strain cases and the iterative algorithms partially successful attempts to traverse the shadowed data.**

Data Location	Image	Comments
$\chi = -121$		Fits peaks from -179 onwards with no difficulty.
$\chi = -19$		The shadowing progresses downwards from $Q$ , the effect upon background can be observed. Signal is diminished.
$\chi = 0$		The most extreme point of the data being obscured. The algorithm fits only the remaining diminished background, no signal at all.
$\chi = 25$		Relevant signal is restored, but the algorithm has not adjusted for the extreme shift in discernable signal.
$\chi = 36$		By $\chi = 30$ , relevant data has begun to fit correctly.

